Stem Cell Reports
Report

ISSCR

OPEN ACCESS

Arginine Methylation Regulates MEIS2 Nuclear Localization to Promote Neuronal Differentiation of Adult SVZ Progenitors

Jasmine Kolb,[1,4] Marie Anders-Maurer,[1] Tanja Müller,[1] Ann-Christin Hau,[1,5] Britta Moyo Grebbin,[1,6] Wiebke Kallenborn-Gerhardt,[2] Christian Behrends,[3,7] and Dorothea Schulte[1,*]

[1]Institute of Neurology, Edinger Institute, University Hospital Frankfurt, 60528 Frankfurt, Germany
[2]Institute of Pharmacology, College of Pharmacy, Goethe University, 60438 Frankfurt, Germany
[3]Institute of Biochemistry II, University Hospital Frankfurt, 60528 Frankfurt, Germany
[4]Present address: Dr. Ehrlich Pharma, 88410 Bad Wurzach, Germany
[5]Present address: Luxembourg Institute of Health, 84 Val Fleuri, 1526 Luxembourg, Luxembourg
[6]Present address: Institute for Tumorbiology and Experimental Therapy, Georg-Speyer-Haus, 60596 Frankfurt, Germany
[7]Present address: Ludwig-Maximilians-Universität München, Munich Cluster of Systems Neurology, 81377 Munich, Germany
*Correspondence: dorothea.schulte@kgu.de
https://doi.org/10.1016/j.stemcr.2018.03.010

SUMMARY

Adult neurogenesis is regulated by stem cell niche-derived extrinsic factors and cell-intrinsic regulators, yet the mechanisms by which niche signals impinge on the activity of intrinsic neurogenic transcription factors remain poorly defined. Here, we report that MEIS2, an essential regulator of adult SVZ neurogenesis, is subject to posttranslational regulation in the SVZ olfactory bulb neurogenic system. Nuclear accumulation of MEIS2 in adult SVZ-derived progenitor cells follows downregulation of EGFR signaling and is modulated by methylation of MEIS2 on a conserved arginine, which lies in close proximity to nested binding sites for the nuclear export receptor CRM1 and the MEIS dimerization partner PBX1. Methylation impairs interaction with CRM1 without affecting PBX1 dimerization and thereby allows MEIS2 nuclear accumulation, a prerequisite for neuronal differentiation. Our results describe a form of posttranscriptional modulation of adult SVZ neurogenesis whereby an extrinsic signal fine-tunes neurogenesis through posttranslational modification of a transcriptional regulator of cell fate.

INTRODUCTION

Postnatal neurogenesis contributes to homeostasis and plasticity in the adult brain by the addition of new neurons and the replacement of old ones in existing network circuitries. In the mammalian forebrain, adult generation of neurons is restricted to few privileged areas, including the subventricular zone (SVZ) and the dentate gyrus (DG) of the hippocampus. The SVZ harbors astroglial-like stem cells, which generate transient amplifying progenitor cells (TAPs) that, after few cell divisions, mature into neuroblasts. Whereas TAPs can still generate both neurons and glia, neuroblasts are committed to the neuronal lineage and already possess traits of immature neurons, such as staining positive for the microtubule-associated protein doublecortin (DCX), the neuron-specific class III β-tubulin (recognized by the TuJ1 antibody), or the polysialylated form of neural cell adhesion molecule (PSA-NCAM). In rodents, SVZ-generated neuroblasts migrate into the olfactory bulb (OB) where they differentiate mostly into inhibitory olfactory interneurons (Hsieh, 2012; Ming and Song, 2011). Continuous SVZ neurogenesis is crucial for the structural and functional integrity of the adult OB and for olfaction-associated behavior (Imayoshi et al., 2008; Sakamoto et al., 2011). In contrast to the developing brain, where the generation of neuronal cell types follows a stereotypic spatial and temporal order, adult neurogenesis is strongly influenced by environmental signals. Examples include the increased generation of granule cells in the DG after physical activity or the modulation of adult SVZ neurogenesis by hormonal changes or in response to hypothalamic innervation (Kempermann et al., 1997; Paul et al., 2017; Shingo et al., 2003). Adult neural stem and progenitor cells thus activate intrinsic neurogenic programs in response to extrinsic signals, which reflect the physiological state of the organism. The molecular pathways by which niche-derived signals are relayed onto transcriptional regulators of cellular differentiation, however, are still poorly defined.

MEIS (myeloid ectopic viral integration site) family proteins belong to the atypical TALE class of homeodomain-containing transcription factors. They function as part of heteromeric complexes with the related PBX (pre-B cell leukemia homeobox) proteins and act synergistically with other transcriptional regulators, including HOX and PAX proteins (Ladam and Sagerström, 2014; Longobardi et al., 2014; Schulte, 2014). In the SVZ, neuronal differentiation requires MEIS2, as *Meis* knockdown or transduction of a function-blocking protein enhanced gliogenic differentiation at the expense of neurogenic differentiation *in vitro* and *in vivo* (Agoston et al., 2014). Mechanistically, MEIS2 recruits the histone modifier PARP1/ARTD1 to transcriptionally inactive, but PBX1-prebound sites in the regulatory regions of neuron-specific genes, thereby facilitating

poly-ADP ribosylation of the linker histone H1 at these sites, which is followed by local decompaction of the chromatin fiber and effective gene expression (Hau et al., 2017). MEIS2-mediated recruitment of PARP1 to chromatin hence constitutes an important early step in the *de novo* activation of neuron-specific genes. Surprisingly, *Meis2* transcripts are already present in quiescent adult neural stem cells in the SVZ, whereas robust MEIS2 immunoreactivity is first seen in neuroblasts (Agoston et al., 2014; Beckervordersandforth et al., 2010). MEIS2 must therefore be under particularly stringent posttranscriptional or posttranslational control in the SVZ, yet the underlying mechanisms are still largely unknown.

RESULTS AND DISCUSSION

MEIS2 Subcellular Localization in SVZ-Derived Progenitor Cells Is Regulated by EGFR Signaling

Adult SVZ-derived stem cells and TAPs grown as primary, free-floating neurospheres (aNS) in the presence of epidermal growth factor (EGF) and basic fibroblast growth factor (FGF2) already possess high levels of *Meis2* transcripts, which increase further during neuronal differentiation, but only faint MEIS2 immunoreactivity (Figures 1A, 1B, and S1). Notably, MEIS2 protein in these cells is evenly distributed between cytoplasm and nucleus, as observed with antibodies directed against different epitopes of the MEIS2 protein (Figures 1B and 1C). In the SVZ *in vivo*, most TAPs (identified as bromodeoxyuridine-positive (BrdU+) cells following a short BrdU pulse or by the Ki67 antigen) also exhibited weak nucleo-cytoplasmic MEIS2 staining (Figures 1D and S1). By contrast, adult SVZ stem cells isolated by their co-expression of GFAP and prominin or putative stem cells *in vitro* (defined as label-retaining, nestin-positive aNS cells, pulse labeled with carboxyfluorescein diacetat succinimidyl ester) are MEIS2 immunonegative (Beckervordersandforth et al., 2010; Figure S1). When SVZ-derived aNS cells were induced to differentiate by removal of EGF and FGF2 from the culture medium and plating on laminin, MEIS2 protein rapidly localized to the nucleus of some cells in the cultures, and these cells began to stain positive for the early neuronal marker PSA-NCAM (Figure 1C). Accumulation of MEIS2 in the cell nucleus is thus a very early sign of neuronal differentiation.

Activated stem cells and proliferating TAPs express EGF receptor (EGFR), and EGFR activation promotes proliferation and counteracts neuronal differentiation *in vivo* and *in vitro* (Doetsch et al., 2002). We therefore induced cellular differentiation in aNS by adding the EGFR inhibitor Tyrphostin AG1478 to EGF/FGF2-containing culture medium and assessed MEIS2 nucleo-cytoplasmic redistribution 8 hr later (Figures 1F–1H and S1). Cells in which nuclear MEIS2 immunoreactivity predominated over that in the cytoplasm were defined as "nuclear accumulation" (e.g., arrowheads in Figures $1C_2$–$1C_4$, middle panels), and cells with uniform MEIS2 staining in cytoplasm and nucleus upon differentiation were counted as "cytoplasmic retention" (e.g., arrows in Figures $1C_2$ and $1C_3$). Treatment with AG1478 elevated the proportion of cells in which MEIS2 accumulated in the cell nucleus 10-fold, while treatment with the FGFR1 inhibitor SU5402 did not (Figures 1F–1H). We concluded that MEIS2 subcellular localization is regulated in response to EGFR signaling.

Neuronal Differentiation Requires Nuclear Accumulation of MEIS2

In silico analysis of the MEIS2 polypeptide sequence identified a nuclear localization signal (NLS) (amino acids 274–280 of NCBI CAA04139.1) and a canonical nuclear export signal (NES) (amino acids 161–163), suggesting that MEIS2 continuously shuttles between nucleus and cytoplasm (Figure 2A). The nuclear accumulation of MEIS2 that accompanies neuronal differentiation must hence involve activation of the NLS and/or silencing of the NES. Remarkably, the NES is fully embedded in a previously identified binding surface for the MEIS dimerization partner PBX (Figure 2A, Knoepfler et al., 1997). We therefore hypothesized that PBX and the nuclear export receptor CRM1 may compete for binding to MEIS2, and that this competition may regulate MEIS2 subcellular localization. We blocked CRM1-dependent nuclear export with leptomycin B (LMB) in aNS grown in EGF/FGF2-containing medium. Eight hours of LMB treatment significantly induced nuclear accumulation of MEIS2 (Figures 2B–2D; 8 hr LMB: 3.33% ± 0.87%, ctrl: 1.22% ± 0.81%). Strikingly, LMB treatment also induced the generation of neurons in these cultures, evident in a more than 3-fold increase in cells labeling for TuJ1 (8 hr LMB: 2.75% ± 0.91%, ctrl: 0.85% ± 0.28%; Figures 2E–2G). Neurogenesis thus occurred despite the fact that the cells were grown in the presence of EGF and FGF2, and hence under conditions that normally preclude cellular differentiation. Adult SVZ-derived progenitor cells thus exist in a delicate "meta-stable" state, which is maintained by the continuous CRM1-dependent export of differentiation-inducing protein(s) from the nucleus. To investigate whether MEIS2 is such a protein, we transduced *Meis2,* C-terminally fused to a triple HA tag and either the strong NLS from SV40 large T antigen or the NES from the HIV tat protein into aNS, induced cellular differentiation 48 hr later, and scored the fate of the transduced cells after 3 days (Figure 2H). Forced nuclear import of MEIS2 increased, whereas forced nuclear export decreased neuron production in these cultures relative to wild-type (WT) MEIS2 (TuJ1+ cells: WT *Meis2* 13.30% ± 3.26%, *Meis2-NES* 5.17% ± 2.71%, *Meis2-NLS* 22.85% ± 2.87%; Figure 2I).

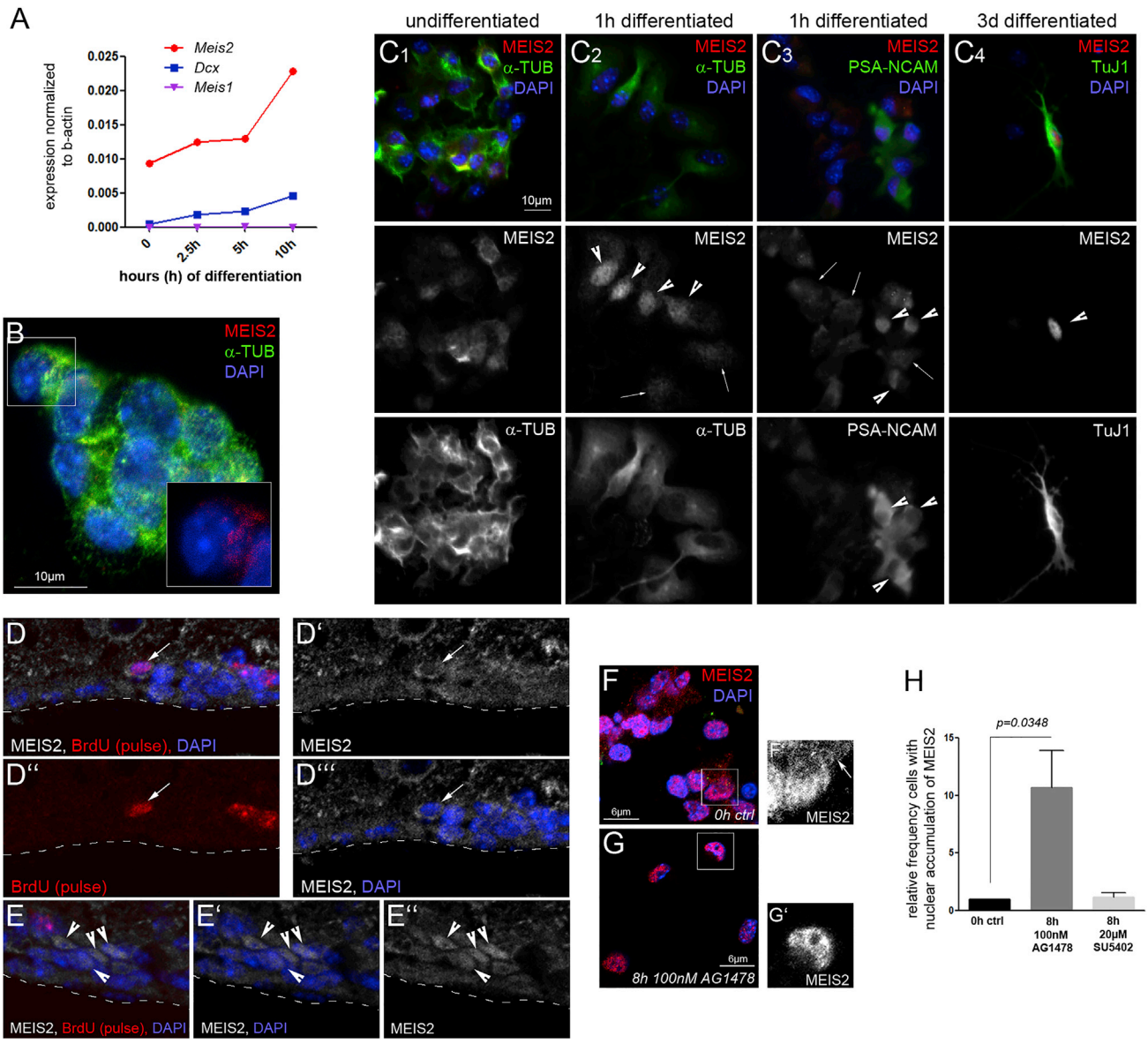

Figure 1. MEIS2 Protein Stability and Subcellular Localization in SVZ-Derived Progenitor Cells Is Controlled by EGFR Signaling

(A) Transcript levels (determined by qPCR) of *Meis1*, *Meis2*, and *Dcx* in primary aNS after induction of neuronal differentiation for the times indicated.

(B) Primary, free-floating aNS stained for MEIS2 (red) and α-tubulin (green); MEIS2 immunoreactivity in cells of the boxed area is shown as insert.

(C) Expression of MEIS2 relative to α-tubulin or the neuron-specific markers PSA-NCAM and TuJ1 in undifferentiated primary aNS, after 1 hr or 3 days of differentiation; arrowheads indicate nuclear accumulation of MEIS2 (middle panel) or PSA-NCAM staining (lower panel); arrows indicate uniform cellular MEIS2 distribution typical of progenitor cells. Scale bars, 10 μm (applies to all panels).

(D and E) Weak, uniform MEIS2 staining in BrdU pulse-labeled TAPs in the SVZ *in vivo*; the arrows in (D) indicate a BrdU-positive cell with MEIS2 cytoplasmic staining; the arrowheads in (E) indicate BrdU-negative, MEIS2-positive putative chain-migrating neuroblasts; BrdU, red; MEIS2, white.

(F and G) Eight hours of treatment with AG1478 (F), but not DMSO as control (G), induces nuclear accumulation of MEIS2 in primary aNS growing in the presence of EGF/FGF2.

(H) Quantification of the results for AG1478, SU5402, and DMSO; n = 3 independent experiments. Data are represented as means ± SEM. See also Figure S1.

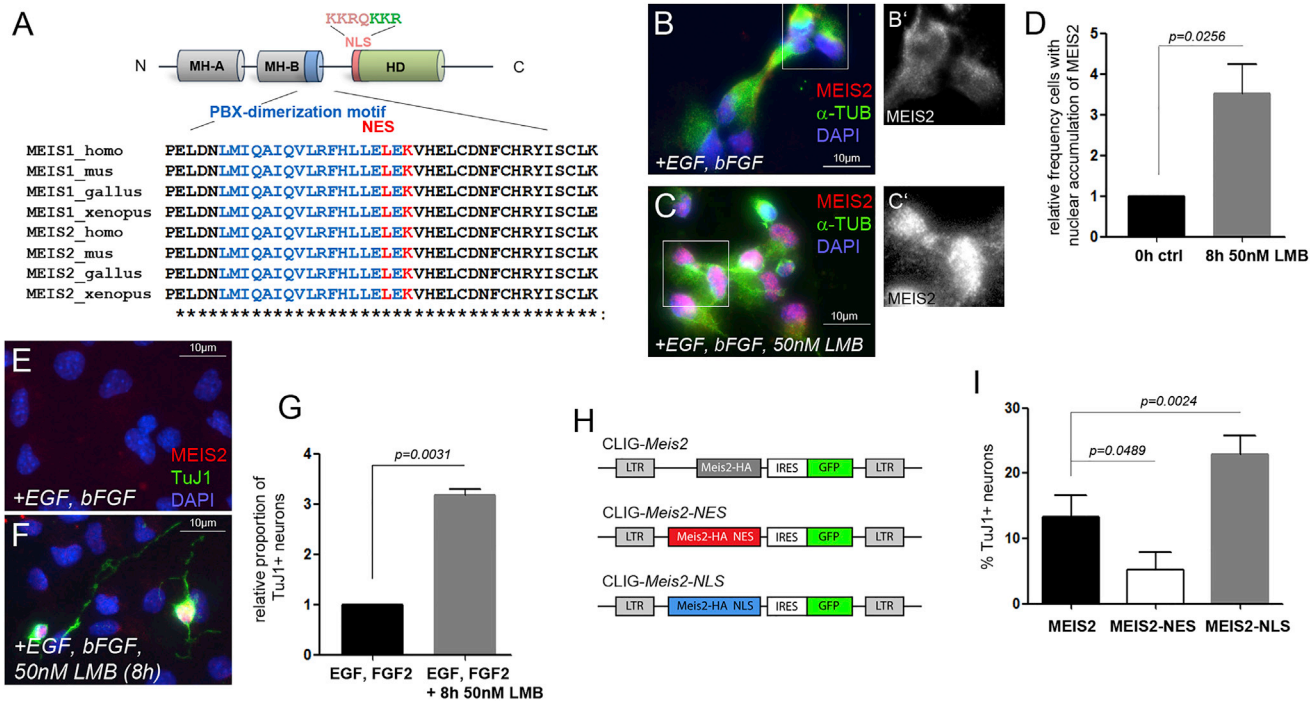

Figure 2. Neuronal Differentiation Requires Nuclear Accumulation of MEIS2

(A) Sequence and relative location of the PBX-interacting motif, NES, and NLS found in Meis family members in different vertebrate species.

(B and C) Subcellular localization of MEIS2 in primary aNS without LMB (B) or treated with LMB (C); MEIS2 immunofluorescence of the boxed areas is shown as single channel in (B′ and C′).

(D) Quantification of the results; n = 5 independent experiments.

(E and F) Inhibition of nuclear export by LMB (F) induces neuronal differentiation in aNS growing in EGF/FGF2-containing medium.

(G) Quantification of the results; n = 3 independent experiments.

(H) Schematic representation of the retroviral vectors used in (I).

(I) Retroviral transduction of *Meis2-NLS* enhances, whereas transduction of *Meis2-NES* reduces neurogenesis relative to WT-*Meis2* (n = 4 independent experiments).

Data in (D), (G), and (I) are represented as means ± SEM. See also Figure S2.

Availability of MEIS2 in the cell nucleus is therefore a rate-limiting determinant of neuronal differentiation of adult SVZ-derived neural progenitor cells.

Although MEIS proteins usually function as components of larger protein complexes, requirement for an otherwise essential binding partner can be overcome by fusion of MEIS to a dominant transactivation domain (Mamo et al., 2006; Wang et al., 2006). Because MEIS2 and PAX6 co-operate in SVZ neurogenesis, we reasoned that *Meis2* fused to the VP16 transactivation domain together with an NLS (*Meis2-VP16-NLS*) may mimic the combined activities of nuclear MEIS2 and PAX6. Indeed, retroviral transduction of *Meis2-VP16-NLS* into free-floating aNS induced massive generation of neurons even in EGF/FGF2-containing medium (Figure S2). When localized to the cell nucleus and in conjunction with a strong transactivation domain, MEIS2 is thus able to direct neurosphere-derived cells toward neurogenesis under conditions that normally preclude neuronal differentiation.

PBX1 and CRM1 Compete for Binding to MEIS2

We directly compared recombinant PBX1 and CRM1 for binding with a synthetic peptide comprising the PBX1-binding motif and NES of MEIS2 (amino acids 146–180 of NCBI CAA04139.1) (Figure 3A). Immobilized peptides were incubated with PBX1 or CRM1, produced by *in vitro* transcription/translation. Both CRM1 and PBX1 were enriched by the peptide with CRM1 binding affinity exceeding that of PBX1 (Figure 3A). Pre-incubation of the peptide with *in vitro*-translated PBX1 blocked CRM1 binding to MEIS2$^{146-180}$, even when excessive amounts of CRM1 were added to the reaction (Figure 3B). CRM1 thus fails to recognize the NES in a PBX1-MEIS2 heterodimer.

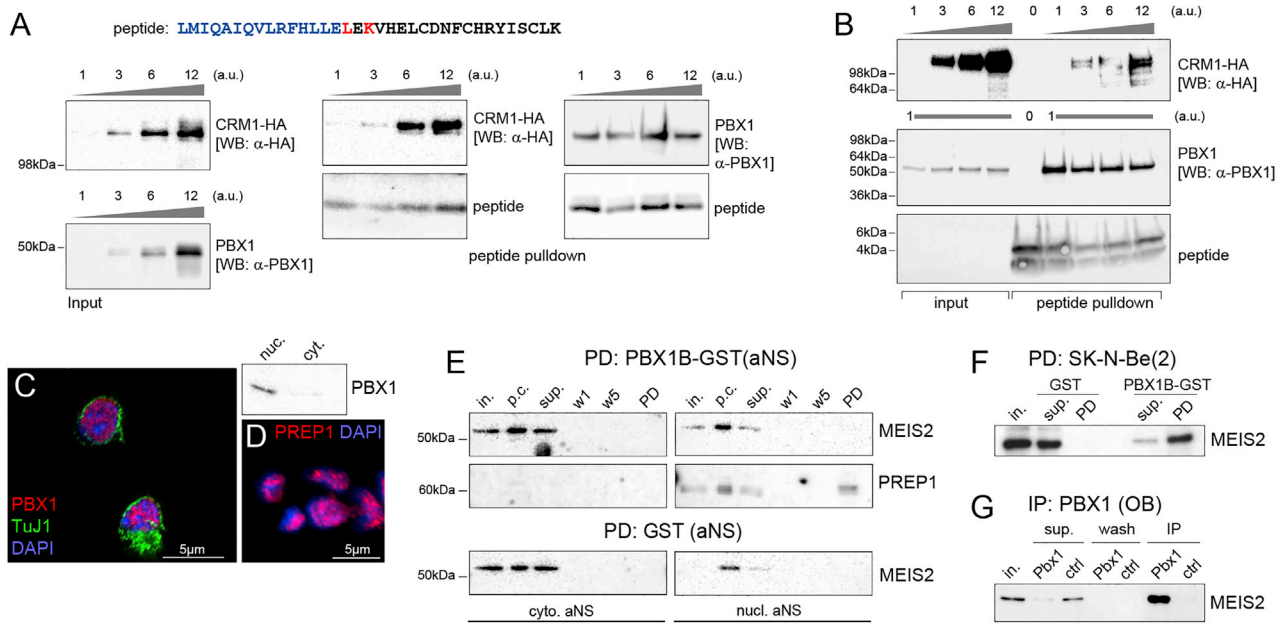

Figure 3. PBX1 and CRM1 Compete for Association with MEIS2

(A) *In vitro* pull-down (PD) assays with synthetic MEIS2 peptides; (left) input: *in vitro*-translated CRM1-HA or PBX1; band intensities correspond to 30% of the protein used for the PD; (middle) PD with CRM1; (right) PD with PBX1. Lower bands: biotinylated peptide eluted from the streptavidin-coated beads. Peptide sequence: PBX dimerization motif, blue; NES, red.

(B) Competitive *in vitro* pull-down assay with MEIS2$^{146-180}$ peptides that were pre-incubated with constant amounts of *in vitro*-translated PBX1 followed by addition of increasing amounts of *in vitro*-translated CRM1-HA.

(C and D) PBX1 (C) and PREP1 (D) are nuclear in primary aNS.

(E) PBX1-GST precipitates PREP1, but not MEIS2, from aNS extracts.

(F) MEIS2 co-precipitates with PBX1-GST from nuclear extracts of SK-N-Be(2) cells.

(G) Co-immunoprecipitation of PBX1 and MEIS2 from the OB. in, input; p.c., preclear; sup., supernatant; w, wash; PD, precipitate of the pull-down; IP, immunoprecipitate; ctrl., isotype-specific control.

Binding of PBX1 to either MEIS or PREP induces nuclear localization of the heterodimer in different physiological contexts (Berthelsen et al., 1998; Mercader et al., 1999). We therefore focused on MEIS-PBX dimer formation. In primary adult SVZ-derived aNS, *PBX1*, *PREP1*, and *MEIS2* are co-expressed, yet only PBX1 and PREP1 localize to the cell nucleus, suggesting that PBX1 may exclusively dimerize with PREP1 in these cells (Figures 3C and 3D). Indeed, pull-down experiments with GST-tagged PBX1 and protein extracts prepared from the nuclear or cytoplasmic compartment of primary aNS enriched PREP1, but not MEIS2 (Figure 3E). Yet, MEIS2 was readily precipitated by PBX1-GST from extracts of SK-N-Be(2) cells or in complex with PBX1 by immunoprecipitation from extracts of adult OB neurons, two cell populations in which MEIS2 localizes to the cell nucleus (Figures 3F and 3G).

Differential Methylation of Arginine 174 Modulates MEIS2 Association with CRM1 or PBX1

We purified MEIS2 from primary SVZ-derived aNS and primary OB tissue and examined both protein fractions by mass spectrometry (MS) (Figures 4A and 4B). Interestingly, MEIS2 purified from the OB but not from aNS carried a mono-methylation on a conserved arginine at position 174 (R^{174}; Figures 4A and 4B). R^{174} lies in close proximity to the overlapping NES- and PBX1-binding motifs, raising the possibility that methylation at this position may regulate MEIS2 nucleo-cytoplasmic localization by altering its affinity toward PBX1 or CRM1 (Figure S3). To test this hypothesis, we first induced primary aNS to differentiate for 4 hr in the presence or absence of adenosine-2′,3′-dialdehyde (AdOX), a general inhibitor of protein arginine methyltransferases (PRMTs). Whereas MEIS2 largely accumulated in the nucleus in control-treated cultures, strong cytoplasmic MEIS2 staining was seen in AdOX-treated cells (Figures 4C–4E). Inhibition of arginine methylation thus prevented the nuclear accumulation of MEIS2 that normally accompanies neuronal differentiation. To investigate whether methylation on R^{174} was involved, we misexpressed HA-tagged MEIS2 or a mutant form of MEIS2 in which R^{174} was replaced with alanine (MEIS2^{R174A}) in aNS. Nuclear accumulation of MEIS2^{R174A} was severely

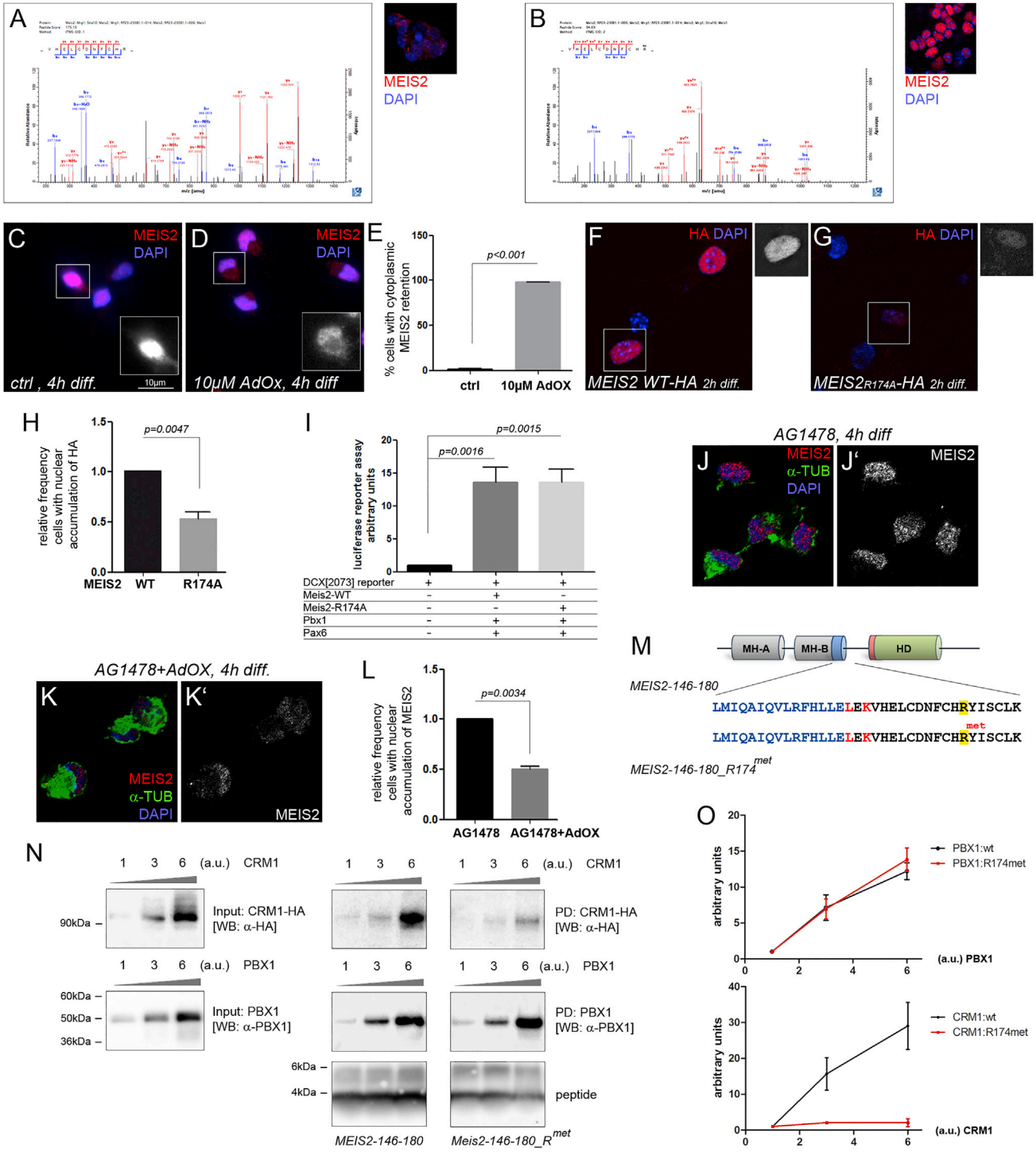

Figure 4. Methylation on R^{174} Modulates CRM1 Binding and Nuclear Localization of MEIS2

(A and B) MS/MS spectra of peptides derived from MEIS2 isolated from aNS (A) and OB (B), methyl modifications at R174 indicated by "me" (B); the inlets show non-nuclear and nuclear MEIS2 immunoreactivity in SVZ-derived aNS and OB, respectively.

(C and D) Inhibition of protein methylation by AdOX (D) prevents nuclear accumulation of MEIS2 upon differentiation; (C) control. MEIS2 immunoreactivity in the boxed cells is shown as inserts.

(E) Quantification of the results; n = 3 independent experiments.

(legend continued on next page)

compromised following 2 hr of differentiation compared with WT-MEIS2 (Figures 4F–4H). A reporter construct in which luciferase is expressed under control of the proximal enhancer/promoter of the *DCX* gene is activated by MEIS2 together with PBX1 and PAX6 when used in a reporter assay in HEK293T cells (Agoston et al., 2014). MEIS2^{R174A} was fully functional in this assay, demonstrating that post-translational modification on R^{174} influences the subcellular localization of the protein but not its ability to activate transcription (Figure 4I). Because EGFR inhibition by AG1478 had been sufficient to induce nuclear localization of MEIS2 in free-floating aNS (Figure 1), we treated aNS with AG1478 together with AdOX, reasoning that AG1478-induced nuclear accumulation of MEIS2 might be precluded by AdOX if R^{174} methylation was occurring as a result of EGFR pathway inhibition. Indeed, significantly fewer cells exhibited nuclear accumulation of MEIS2 after 4 hr of combined treatment with AG1478 and AdOX than after treatment with AG1478 alone (AG1478: 5.52% ± 1.8%; AG1478 + AdOX: 2.7% ± 0.9%; Figures 4J–4L). Collectively, these observations argue that the nucleo-cytoplasmic redistribution of MEIS2 upon EGFR pathway inhibition acts via differential methylation of MEIS2 on R^{174}. We therefore directly compared recombinant PBX1 and CRM1 for binding with synthetic peptides that were either non-methylated (MEIS2$^{146-180}$) or methylated on R^{174} (MEIS2$^{146-180met}$; Figure 4M). Whereas PBX1 alone co-precipitated equally well with the methylated and non-methylated peptide, CRM1 bound more strongly to MEIS2$^{146-180}$ than to MEIS2$^{146-180met}$ (Figures 4N and 4O). Methylation at R^{174} thus reduces MEIS2 affinity for CRM1 and thereby indirectly favors its association with PBX1.

In sum, nuclear localization of a MEIS family protein and its ability to dimerize with PBX can be jointly regulated by methylation on an evolutionary conserved arginine residue. Although it is well established that nuclear localization of PBX1 or its *D. melanogaster* homolog *extradenticle* (*exd*) requires association with an MEIS family dimerization partner (Abu-Shaar et al., 1999; Berthelsen et al., 1999), the results presented here establish an additional level of complexity by demonstrating that the subcellular localization of MEIS itself is modulated by posttranslational modification as a function of cellular differentiation. In addition, our results provide evidence for a mode by which adult SVZ neurogenesis can be quickly fine-tuned in response to extracellular signals: in adult SVZ progenitor cells, non-methylated MEIS2 is rendered inactive by continuous CRM1-dependent nuclear export. Methylation on R^{174} weakens CRM1 binding to MEIS2 and thereby facilitates MEIS2 dimerization with PBX1 and its accumulation in the cell nucleus, an established prerequisite for neuronal differentiation (Agoston et al., 2014; Hau et al., 2017). On the molecular level, methylation on R^{174} may modulate MEIS2 subcellular distribution either directly by steric interference with CRM1 binding or more indirectly by inducing a conformational change in the MEIS2 polypeptide chain, which then masks the NES. Our observation that methylation on R^{174} decreased binding of CRM1 to the MEIS2 NES in a peptide of only 35 amino acids in length argues that R^{174} methylation directly impacts on CRM1 binding. Notably, *in silico* protein structure predictions indicate that the MH-B domain of MEIS2, harboring the PBX-binding motif, NES, and R174, forms an α-helical secondary structure in solution, which condenses the 11 amino acid distance between R^{174} and the NES to three helical turns, bringing R^{174} and the NES in even closer proximity (Figure S3).

Because inhibition of PRMTs by AdOX counteracted the nuclear accumulation of MEIS2, which is normally induced by AG1478 treatment, EGFR pathway inhibition likely plays a major role in R^{174} methylation of MEIS2.

(F and G) Subcellular localization of HA-tagged WT-MEIS2 (F) and MEIS2-R174A (G) in aNS after 2 hr of differentiation; MEIS2 immunoreactivity in the boxed cells is shown in separate panels.
(H) Quantification of the results; n = 4 independent experiments.
(I) Luciferase reporter assay in HEK293T cells: a 2073 basepair fragment of the murine *DCX* promoter/proximal enhancer is transcriptionally activated by PBX1 and PAX6 together with WT-MEIS2 or MEIS2^{R174A}; n = 7 independent experiments.
(J and K) Subcellular distribution of MEIS2 after 4 hr of treatment with AG1478 alone (J) or in combination with AdOX (K); MEIS2 immunofluorescence is shown as separate panels in (J′ and K′).
(L) Quantification of the results; n = 3 independent experiments.
(M) Amino acid sequence of the methylated and non-methylated MEIS2 peptides.
(N) Different binding affinities of PBX1 and CRM1 to methylated and non-methylated peptides; (left) input: *in vitro*-translated CRM1-HA or PBX1; (middle) PD with non-methylated MEIS2$^{146-180}$; (right) PD with MEIS2$^{146-180}$ methylated on R^{174}. The lower panels show the biotinylated peptide eluted from the streptavidin-coated beads.
(O) Densitometric quantification of the band intensities of PBX1 (left) and CRM1 (right) bound to non-methylated (WT, black) or methylated peptide (R174met, red) as shown in (N); n = 4 independent experiments. PD, precipitate of the pull-down. The lowest band intensity was set as a.u. 1. PBX1 binds with equal affinities to both peptides, whereas CRM1 prefers the non-methylated form.
Data in (E), (H), (I), (L), and (O) are represented as means ± SEM.

Downregulation of EGFR signaling *in vitro* is achieved by removing EGF from the culture medium, an integral step in virtually all *in vitro* differentiation protocols for adult neural stem and progenitor cells. In the SVZ *in vivo*, the process is undoubtedly more complex and likely involves the integration of multiple extracellular signals, possibly together with the spatial displacement of progenitor cells from the influence of the stem cell niche. Irrespective of how EGFR signaling is terminated, the data presented here highlight how extracellular signals can impinge on a transcriptional regulator of neurogenic differentiation.

EXPERIMENTAL PROCEDURES

Experiments Involving Animals and Cell Culture

Sphere-forming cells were isolated from 7- to 10-week-old C57BL6 mice, cultured, and retrovirally transduced following published protocols (Agoston et al., 2014). All procedures involving animals were approved by the local animal care committee and the government of Hessen and are in accordance with German and EU regulations. SK-N-Be(2) and HEK293T cells were cultured following standard conditions. For pharmacological inhibitors, plasmids, and small interfering RNAs, see Supplemental Information.

Retroviral Constructs

Full-length *Meis2b* was C-terminally fused to a triple HA tag and cloned into the retroviral vector pCLIG (Agoston et al., 2014). *Meis2-NLS* and *Meis2-NES* carry oligonucleotides corresponding to the NLS of SV40 large T antigen (PKKKRKV) or the NES of the HIV− tat protein, respectively, inserted in frame in the HA tag of *mMeis2b-HA*. In CLIG-*Meis2-NLS-VP16*, mMEIS2b-HA was C-terminally fused to the SV40 large T antigen NLS followed by an in-frame fusion to the herpes simplex virion protein 16 transactivation domain. In CLIG-*Meis2*-R174A, the arginine at position 174 of mMEIS2B-HA was converted into alanine by site-directed mutagenesis (Phusion Site-Directed Mutagenesis Kit, Thermo Scientific, F-541). Luciferase reporter assays were performed as described in Agoston et al. (2014).

MS Analysis

Peptide mixtures derived from in-gel tryptic digests of SDS-PAGE-separated MEIS2 immunoprecipitates were analyzed by liquid chromatography-tandem MS (LC-MS/MS) using an EasyLC nano-HPLC coupled to an Orbitrap Elite mass spectrometer (both Thermo Scientific). MS raw data were processed by MaxQuant (Cox and Mann, 2008) with methylation of arginine and lysine set as variable modifications.

Peptide Pull-Down

Peptides comprising the sequences LM**I**QAIQV**L**RFH**LL**E**L**EKVH ELCDNFCHRYISCLK and LM**I**QAIQV**L**RFH**LL**E**L**EKVHELCDNF CHR{met}YISCLK, N-terminally linked to a mini-PEG linker followed by biotin (ProteoGenix; Schiltigheim, France), were immobilized on streptavidin-coated Dynabeads (Invitrogen) in 20 mM sodium phosphate (pH 7.4), 150 mM KCl, 0.5 mM EDTA, 5 mM $MgCl_2$, 10% glycerol, cOmplete protease inhibitor cocktail (Roche), washed, blocked with 0.1% BSA, and incubated with different amounts of recombinant PBX1 or CRM1-HA generated by TNT-coupled transcription/translation (Promega) for 2 hr at 4°C. For competitive pull-down assays, peptide-loaded beads were pre-incubated with PBX1 for 30 min prior to the addition of CRM1-HA. Proteins were resolved by SDS-PAGE and detected by western blot with antibodies against PBX1 (Chemicon), hemagglutinin (HA) (Roche) to detect CRM1-HA or horseradish peroxidase-coupled streptavidin to detect the biotinylated peptide. For the quantification shown in Figure 4O, band intensity was determined densitometrically with ImageJ.

SUPPLEMENTAL INFORMATION

Supplemental Information includes Supplemental Experimental Procedures and three figures and can be found with this article online at https://doi.org/10.1016/j.stemcr.2018.03.010.

AUTHOR CONTRIBUTIONS

J.K., M.A.M., T.M., A.C.H., B.M.G., and W.K.G. performed the experiments. C.B. performed MS analysis. D.S. and J.K. designed the study. D.S. wrote the manuscript.

ACKNOWLEDGMENTS

We thank Ralph Kehlenbach (University Medical School Göttingen) and Licia Selleri (University of California, San Francisco) for reagents. The work was supported by the Deutsche Forschungsgemeinschaft (SCHU1218/3-3 to D.S. and BE4685/1-1 to C.B.), the August Scheidel-Foundation, the Schram-Foundation, and the Ludwig Edinger-Foundation.

Received: October 16, 2017
Revised: March 12, 2018
Accepted: March 13, 2018
Published: April 10, 2018

REFERENCES

Abu-Shaar, M., Ryoo, H.D., and Mann, R.S. (1999). Control of the nuclear localization of Extradenticle by competing nuclear import and export signals. Genes Dev. *13*, 935–945.

Agoston, Z., Heine, P., Brill, M., Grebbin, B., Hau, A.-C., Kallenborn-Gerhardt, W., Schramm, J., Götz, M., and Schulte, D. (2014). Meis2 is a Pax6 co-factor in neurogenesis and dopaminergic periglomerular fate specification in the adult olfactory bulb. Development *141*, 28–38.

Beckervordersandforth, R., Tripathi, P., Ninkovic, J., Bayam, E., Lepier, A., Stempfhuber, B., Kirchhoff, F., Hirrlinger, J., Haslinger, A., Lie, D.C., et al. (2010). In vivo fate mapping and expression analysis reveals molecular hallmarks of prospectively isolated adult neural stem cells. Cell Stem Cell *7*, 744–758.

Berthelsen, J., Zappavigna, V., Ferretti, E., Mavilio, F., and Blasi, F. (1998). The novel homeoprotein Prep1 modulates Pbx-Hox protein cooperativity. EMBO J. *17*, 1434–1445.

Berthelsen, J., Kilstrup-Nielsen, C., Blasi, F., Mavilio, F., and Zappavigna, V. (1999). The subcellular localization of PBX1 and EXD proteins depends on nuclear import and export signals and is modulated by association with PREP1 and HTH. Genes Dev. *13*, 946–953.

Cox, J., and Mann, M. (2008). MaxQuant enables high peptide identification rates, individualized p.p.b.-range mass accuracies and proteome-wide protein quantification. Nat. Biotechnol. *26*, 1367–1372.

Doetsch, F., Petreanu, L., Caille, I., Garcia-Verdugo, J.M., and Alvarez-Buylla, A. (2002). EGF converts transit-amplifying neurogenic precursors in the adult brain into multipotent stem cells. Neuron *36*, 1021–1034.

Hau, A.C., Grebbin, B.M., Agoston, Z., Anders-Maurer, M., Müller, T., Groß, A., Kolb, J., Langer, J.D., Döring, C., and Schulte, D. (2017). MEIS homeodomain proteins facilitate chromatin opening through PARP1/ARTD1-mediated eviction of histone H1. J. Cell Biol. *216*, 2715–2729.

Hsieh, J. (2012). Orchestrating transcriptional control of adult neurogenesis. Genes Dev. *26*, 1010–1021.

Imayoshi, I., Sakamoto, M., Ohtsuka, T., Takao, K., Miyakawa, T., Yamaguchi, M., Mori, K., Ikeda, T., Itohara, S., and Kageyama, R. (2008). Roles of continuous neurogenesis in the structural and functional integrity of the adult forebrain. Nat. Neurosci. *11*, 1153–1161.

Kempermann, G., Kuhn, H.G., and Gage, F.H. (1997). More hippocampal neurons in adult mice living in an enriched environment. Nature *386*, 493–495.

Knoepfler, P.S., Calvo, K.R., Chen, H., Antonarakis, S.E., and Kamps, M.P. (1997). Meis1 and pKnox1 bind DNA cooperatively with Pbx1 utilizing an interaction surface disrupted in oncoprotein E2a-Pbx1. Proc. Natl. Acad. Sci. USA *94*, 14553–14558.

Ladam, F., and Sagerström, C.G. (2014). Hox regulation of transcription: more complex(es). Dev. Dyn. *243*, 4–15.

Longobardi, E., Penkov, D., Mateos, D., De Florian, G., Torres, M., and Blasi, F. (2014). Biochemistry of the tale transcription factors PREP, MEIS, and PBX in vertebrates. Dev. Dyn. *243*, 59–75.

Mamo, A., Krosl, J., Kroon, E., Bijl, J., Thompson, A., Mayotte, N., Girard, S., Bisaillon, R., Beslu, N., Featherstone, M., et al. (2006). Molecular dissection of Meis1 reveals 2 domains required for leukemia induction and a key role for Hoxa gene activation. Blood *108*, 622–629.

Mercader, N., Leonardo, E., Azpiazu, N., Serrano, A., Morata, G., Martínez, C., and Torres, M. (1999). Conserved regulation of proximodistal limb axis development by Meis1/Hth. Nature *402*, 425–429.

Ming, G.L., and Song, H. (2011). Adult neurogenesis in the mammalian brain: significant answers and significant questions. Neuron *70*, 687–702.

Paul, A., Chaker, Z., and Doetsch, F. (2017). Hypothalamic regulation of regionally distinct adult neural stem cells and neurogenesis. Science *356*, 1383–1386.

Sakamoto, M., Imayoshi, I., Ohtsuka, T., Yamaguchi, M., Mori, K., and Kageyama, R. (2011). Continuous neurogenesis in the adult forebrain is required for innate olfactory responses. Proc. Natl. Acad. Sci. USA *108*, 8479–8484.

Schulte, D. (2014). Meis: new friends of Pax. Neurogenesis *1*, e976014.

Shingo, T., Gregg, C., Enwere, E., Fujikawa, H., Hassam, R., Geary, C., Cross, J.C., and Weiss, S. (2003). Pregnancy-stimulated neurogenesis in the adult female forebrain mediated by prolactin. Science *299*, 117–120.

Wang, G.G., Pasillas, M.P., and Kamps, M.P. (2006). Persistent transactivation by meis1 replaces hox function in myeloid leukemogenesis models: evidence for co-occupancy of meis1-pbx and hox-pbx complexes on promoters of leukemia-associated genes. Mol. Cell. Biol. *26*, 3902–3916.